PHOTOPHYSICAL PROPERTIES OF AU AND AU@SIO2 NANOPARTICLE-DYE COMPLEXES IN MESOPOROUS SILICA MATRICES FOR THERANOSTICS PURPOSES

K. MATVEEVA[1], A. ZYUBIN[1], A. OGNEDYUK[1], E. DEMISHKEVICH[1], I. KON[1], I. SAMUSEV[1]

[1]Immanuel Kant Baltic Federal University,
Nevskogo St., 14A, 236041 Kaliningrad, Russia
E-mail: matveeva.k.i@inbox.ru

Received May19, 2021

Abstract. This paper summarizes a detailed study of plasmon-enhanced/quenched fluorescence of gold nanoparticles (NP) and rhodamine 6G (R6G) dye complexes. Spectral fluorescent properties of the complexes with/without SiO_2 shell have been investigated. FDTD modeling of optical parameters has been carried out. Mesoporous silica nanoparticles (MSNs) have been added to the system in the case of Au@SiO_2 NPs. The influence of SiO_2 shells and MSNs on the photophysical properties of the complexes studied has been demonstrated.

Key words: gold, core/shell nanoparticles, MEF, quenching, mesoporous silica.

1. INTRODUCTION

In recent decades, 10 ÷ 100 nm gold nanoparticles (NPs) of different forms and shapes [1] have been widely used in many optical and biophysical studies [2] due to localized surface plasmon resonance (LSPR) induced at NPs surface [3]. Such an approach has brought about abundant research of a wide range of biophysical objects: cells and their components [4], enzymes [5], peptides [6], etc. LPSR makes it possible to amplify spectral absorbance [7], fluorescence [8] and scattering [9] signals from low-scattered [10] and low-fluorescent objects in visible [11] and near-infrared regions [12]. Despite the disadvantages of gold colloidal nanoparticles, which include toxicity to biophysical systems, low colloidal stability, thermal and chemical reactivity; spherical gold NPs can be used as sensitive and tuned plasmonic core in multilayered NPs structures [13]. A wide variety of organic and inorganic layers are used to overcome the drawbacks of spherical NPs [13]. Coating shell can enhance colloidal stability, decrease toxicity, and allow for further functionalization of the NP to form a theranostic complex. Inorganic silica (SiO_2) shell is also widely used as capsuling material due to its chemical inertness, optical transparency and excellent shell thickness control [14].

Since Au NPs and Au@SiO_2 NPs can act as energy coupling between free electrons and fluorophores, such structures can be applied for sensor purposes. Both metal-enhanced fluorescence (MEF) and quenching effects for Ag(Au)@SiO_2 NPs have been introduced for optical and biophysical studies [15]. The authors of [16] used steady-state, time-resolved fluorescence spectroscopy and were able to build a theoretical model to evaluate electromagnetic coupling between a fluorophore and a NP. They state that, for quenching, coupling parameters depend on the distance between the fluorophore and the NP within a complex and on the wavelength of the excitation source (in correlation with the LSPR maximum). One paper [17] describes an MEF effect study for Au@SiO_2 core-shell NPs in complex with Oregon Green 488-isothiocyanate dye. The authors varied SiO_2 shell thickness and Au core diameter to achieve 35 times stronger fluorescence emission in comparison with OG-488 doped silica spheres without Au core. Mesoporous silica nanoparticles (MSNs) are widely used for biophysical research as they have significant pore size, optical transparency, and large surface area [18]. Great attention is paid to synthesis, characterization and application of MSNs [19]. When combined with metal NPs (as a shell or with matrices), it becomes possible to quench or amplify fluorescence and use it for sensory purposes with delivery functions [20]. Plasmon processes for Au NPs and NP-based complexes can be evaluated and described with simulation methods, such as the Finite-Difference Time-Domain (FDTD) method, for example [21]. The FDTD method is based on Maxwell's equations which describe electric and magnetic components of electromagnetic waves in interaction with quasi-free charges existing in metallic NPs, and can be used to evaluate electromagnetic field distortion near the surface of metallic NPs [22]. Since silica shell can contribute to scattering, the FDTD method can be applied for calculations of NPs coated with silica shell [23] and coated with a two-layer shell, including a drug model between SiO_2 and Au [24]. On the other hand, a combination of experimental and theoretical approaches based on energy transfer calculations can be applied to NP-dye interactions [25]. For quenching processes, such parameters as quenching constants, binding constants, and thermodynamics can be evaluated [26]. NP-dye complexes can be described in terms of energy transfer. Förster (FRET) and Dexter models [27], nanometal energy transfer model (NSET), as well as plasmon resonance energy transfer (PRET) can be applied as effective optical instruments for energy transfer calculations [28]. Both MEF and quenching can be effectively evaluated in terms of energy transfer processes. This paper reports on the study of plasmon-enhanced/quenched fluorescence in Au and Au@SiO_2 complexes combined with rhodamine 6G (R6G) in MSN NP matrix (for Au@SiO_2). We have experimentally defined NP and R6G concentrations suitable for R6G fluorescence enhancement and quenching. Spectral fluorescence parameters have been found for 20 Au-R6G and 20 Au@SiO_2 complexes. The difference in photophysical properties for Au and Au@SiO_2 in complex with R6G has been demonstrated. For the Au@SiO_2

case, MSN matrix was added to the system to investigate its influence on quenching and MEF processes.

2. EXPERIMENTAL SECTION

2.1. FDTD SIMULATION

Simulation was carried out using the Lumerical FDTD Solutions software package and the algorithm described in detail for three layered core/shell structure in [24]. Simulations were run for Au NPs with size d = 15 nm, core-shell Au@SiO_2 NPs with core size d = 15 nm and shell size d = 18 nm and MSN with d = 18 nm. The counting area, grid resolution, and boundary conditions were set first. In the second step, a body with specified optical and geometric parameters was placed inside the counting area. Material and geometric parameters of the samples were set next. We used materials from Lumerical database (Au, SiO_2) and adopted its parameters (size, form, geometry) for the simulation. The radiation source was set in the third step. The Total-Field Scattered-Field (TFSF) source was used for simulations. The source of time-finite electromagnetic wave monitor was set next. We used frequency domain field 2D monitors that collected the frequency domain field profile and provided spatial domain simulations to the FDTD solver. Under laser excitation near the absorption maximum, a metal NP (including core-shell structure) produces localized surface plasmon and surface plasmon polariton (SPP). The size of the counting region was set at the highest possible resolution with a minimum step of 0.25 nm. Excitation was performed by a plane wave polarized along the z axis according to the TFSF method, in which the total field is decomposed into an incident field and a scattered field. The following standard modeling parameters were used: travel time of a plane-polarized wave through the working area was set to 1000 fs and a temperature of 300 K. As a result, E values for Au and Au@SiO_2 NPs were calculated.

2.2. SYNTHESIS OF AU NPS, AU@SIO2 NPS, MSNS

Chemically pure reagents and Milli-Q water (18.2 MΩ.cm) were used for all experiments. Synthesis protocol was based on [29] with modification to only achieve spherical NPs as the end product of the synthesis. Seed solution was prepared as a first step as follows: 500 µl of 0.0137 M cetyltrimethylammonium bromide (CTAB, AppliChem) solution was mixed with 20 µl of 0.01 M $HAuCl_4$ (Aurat Ltd.). 100 µl of freshly prepared NaBH4 (Lenreactiv Ltd.) was added next and shaken vigorously for 1 min. After adding $NaBH_4$, the color of the seed solution changed from slightly yellow to yellowish brown. The seed solution needed to be used within 30 minutes to 2 hours after preparation to avoid sample

"aging", which usually reveals itself as a color change from yellowish brown to pink. In the second step, spherical Au NPs were prepared as follows: 9.5 ml of 0.0137 M CTAB was mixed with 10 μl of 0.004 M aqueous $AgNO_3$ solution. 750 μl of 0.01 M of $HAuCl_4$ was added next, followed by 100 μl of 0.08 M ascorbic acid. The solution was then mixed by inverting the tube several times, its resulting color changing from dark yellow to milky white. Finally, 36 μl of seed solution was added. The color change occurred almost immediately to pinkish and became bright red over several following hours. In order to form SiO_2 and MSNs, 10 ml of Au NPs was brought to 10 - 11 pH value by adding of 20% NaOH. Then, based on [29], with constant stirring at 70 rpm, a TEOS (Sigma-Aldrich)/EtOH (Chimmed Ltd.) solution with a ratio of 20 μL/190 μL was added dropwise. After 1 h and 2 h, another 20 μL was added consistently. The stirring speed was increased to 800 rpm. In order to form MSNs and SiO_2 shells on Au NPs, after 4 h and 6 h, another 200 μL of TEOS was added. To form the SiO_2 shells and dispersed MSNs, stirring continued for 20-24 hours. After preparation, $AuSO_2$ with MSNs were stored for further experiments.

2.3. FORMATION OF AU NPS-R6G AND AU@SIO_2-R6G COMPLEXES

Rhodamine 6G (R6G) solutions with concentrations of 1000, 100, 10, and 1 μM were prepared for complexes study. Au NPs and Au@SiO_2 NPs with concentration ranging from 0.1 nM to 1 μM and 1 nM to 0.1 μM were prepared by diluting the stock solution of 1 μM R6G ten times. 20 Au-R6G and 20 Au@SiO_2 complexes in MSN were prepared for the study.

2.4. SPECTROPHOTOMETRY (UV/VIS SPECTROSCOPY)

Absorption spectra of Au NPs, Au@SiO_2 NPs were registered using UV/Vis absorption spectrophotometer UV-2600 (Shimadzu, Japan). 4 ml of the sample was placed in a polymer cuvette optically transparent in visible range (300 ÷700 nm) and then in the unit holder. Registration was carried out within 200 ÷ 800 nm wavelength range. Spectral data were collected and saved in .txt format for further processing.

2.5. DYNAMIC LIGHT SCATTERING (DLS)

Dynamic light scattering for Au NPs, Au@SiO_2 NPs was performed with Photocor Complex spectrometer (Photocor Ltd., Russia). The cuvette with the sample was placed in the sample holder of the analyzer. Laser radiation at 432 nm was passed through the NPs solution and then scattered on NPs. The scattered light was detected by the photon counting system and the output signal was transferred

to the correlator input. The correlator accumulated function of the scattered light intensity fluctuation. DynaLS software was used to calculate the NPs size from the correlation function. NPs size was calculated for all Au and Au@SiO_2 samples. The size of Au NPs was calculated to be d = 15 nm and size of Au@SiO_2 NPs with MSM was calculated to be d = 18 nm.

2.6. SCANNING ELECTRON MICROSCOPY

Morphology and size were investigated for Au NPs and Au@SiO_2 NPs in MS matrix with a Carl ZEISS Crossbeam 540 electron microscope. Next, sample drops were dried in vacuum and placed in the unit holder on silicon substrate. SEM images were collected with 1 nm spatial resolution.

2.7. SPECTROFLUORIMETRY

Fluorescence of Au-R6G and Au@SiO_2-R6G complexes was studied using the Fluorolog-3 spectroflurimeter (Horiba, Japan). Excitation was carried out by a 450 W xenon lamp, applied as a source of broadband continuous radiation. Excitation was set at wavelength λ_{ex} = 520 nm corresponding to both R6G absorption and Au plasmon absorption peaks. The samples were placed separately in a quartz cuvette and then in the sample holder. The light flux passed through a double excitation monochromator equipped with 1200 gr/mm grating according to the Czerny-Turner scheme. The blaze angle was optimized for the visible region (400 ÷ 500 nm). After interaction with the sample, according to the Cherni-Turner scheme, the light flux passed to the detector through a double monochromator with a flat diffraction grating with angle optimized for the visible region (500 nm). After that, the fluorescence spectrum of the sample was recorded in the .txt format to be further processed using the Origin Pro software.

3. RESULTS AND DISCUSSION

One of the ideas of this paper was to form silica matrixes with MSNs. Figure 1 displays the SEM image for the CTAB capped Au NPs on Si substrate. Gold NP aggregations and single NPs with the average size of d = 15 nm (Fig. 1, inset) can be seen on the surface. For Au@SiO_2 in MSNs matrix, the average size for both types of NPs was detected as d = 18 nm (Fig 2, inset). As for the distribution, one can see that the NPs were more dispersed in this case. Au@SiO_2 NPs were integrated in MSNs matrix (Fig.2). SEM images demonstrate high concentration of MSNs matrix on Si surface, which can have a positive effect on the drug load inside the matrix.

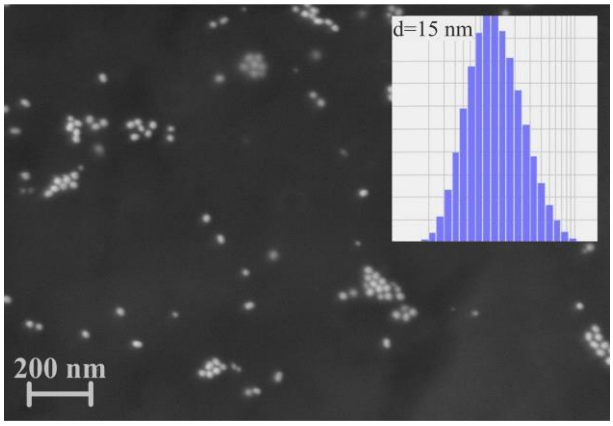

Fig. 1 – SEM image of Au with size distribution in colloid solution (inset).

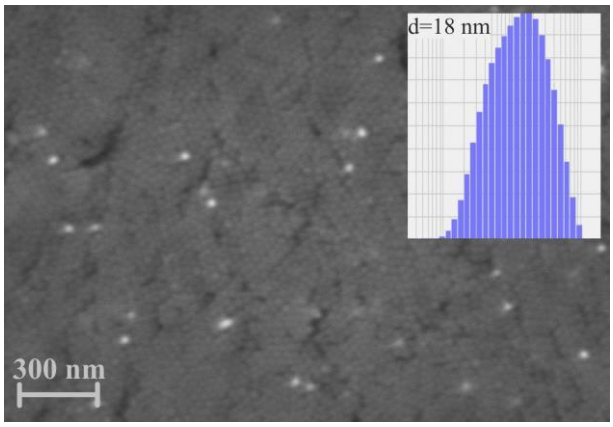

Fig. 2 – SEM image of $Au@SiO_2$, MSNs with size distribution in colloid solution (inset).

Figure 3 shows the results of studies of the absorption spectra for Au NPs (Fig.3, red line) and for $Au@SiO_2$ in MSN matrix (Fig.3, violet dotted line). It can be seen that, in $Au@SiO_2$ with MSNs, absorption is 1.51 times stronger than in Au without SiO_2. This occurs due to the deposition of a silicon shell on gold nanospheres [30].

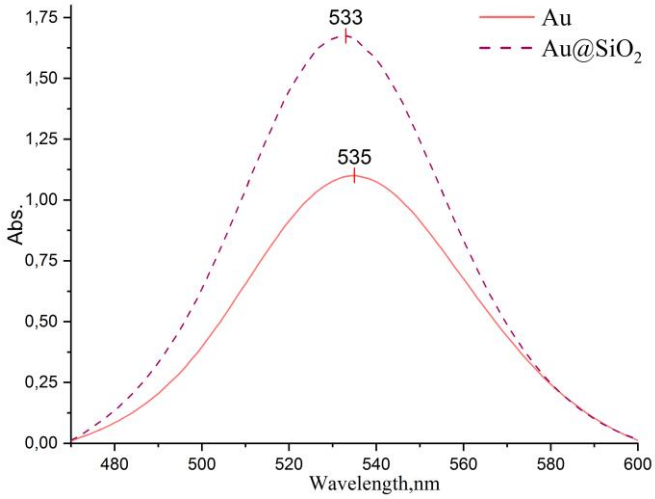

Fig. 3 – (Color online) Absorption spectra for Au NPs (red line) and for Au@SiO_2 in MSN matrix (violet dotted line).

FDTD results (Figures 4 – 6) demonstrate an increase in electromagnetic distortion for Au@SiO_2 NPs (E_{max} = 5.8 V/m) in comparison with Au NPs (E_{max} = 4.6 V/m). MSNs without Au core provides E_{max} = 3.9 V/m enhancement. This can explain the increase in NPs absorption for the violet dotted line (Fig. 3). However, since average shell thickness is 3 nm, no red shift was observed in the UV/Vis absorption spectra and none according to the photon correlation spectroscopy data. On the contrary, a weak blue 2 nm shift occurred in Au@SiO_2 in MSN matrix absorption spectra, which can be explained by the scattering of [31] MSN matrix.

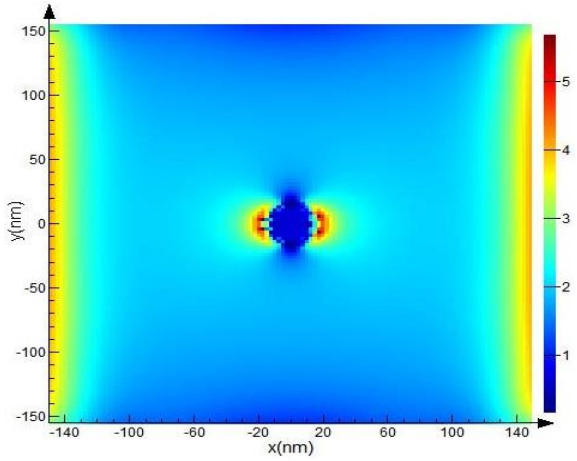

Fig. 4 – (Color online) FDTD simulation results for Au@SiO_2 NPs of d=18 nm size.

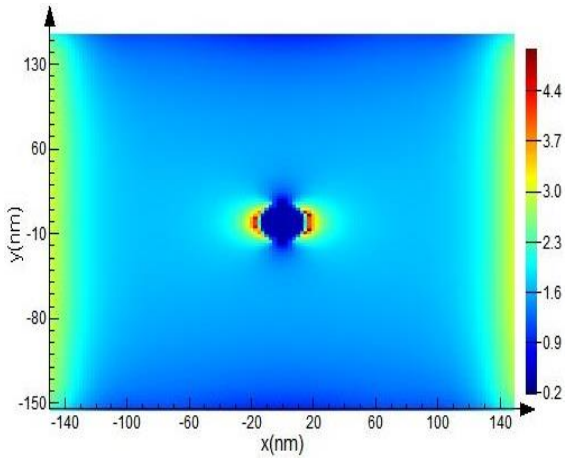

Fig. 5 – (Color online) FDTD simulation results for Au NPs with d=15 nm size.

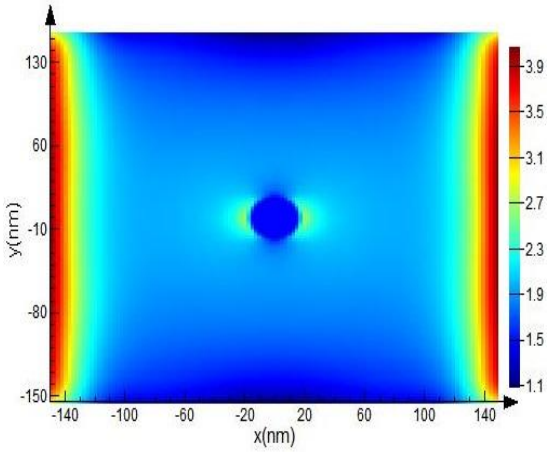

Fig. 6 – (Color online) FDTD simulation results for MSNs with d=18 nm size.

The calculation of the molar concentration of nanoparticles was performed according to the following formula [32]:

$$C = \frac{6MN_{Total}}{\pi d^3 \rho V N_a} \quad (1)$$

where ρ is the density of face-centered cubic gold (g/cm^3); d is an average diameter of NPs (nm); M is the atomic weight of gold; N_{Total} is the total number of gold atoms added

as $HAuCl_4$; V is the volume of the reaction solution (L); and N_a is the number of atoms per mole (Avogadro's constant = $6.023 \cdot 10^{23}$).

Figures 7 – 10 show the fluorescence spectra of Au-R6G complexes for four R6G concentrations varied from 1 μM to 1 mM. Both MEF and quenching processes were detected for all four R6G concentrations. The obvious red shift of 8 nm was detected for the sample with 2.2 μM Au concentration. The shift decreased with lower Au NPs concentration. The other shift caused by high R6G concentrations due to complex formation between R6G molecules was not detected.

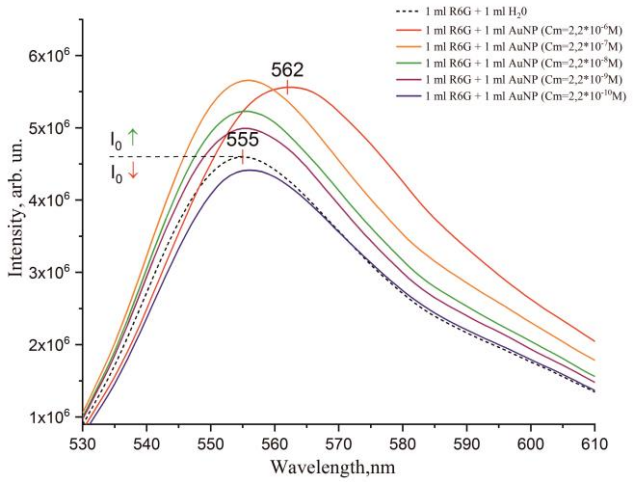

Fig. 7 – (Color online) Fluorescence spectra of the R6G-Au NPs complex where Au NPs are spherical, molar concentration of NPs is variable and R6G concentration is constant at 1000 μM.

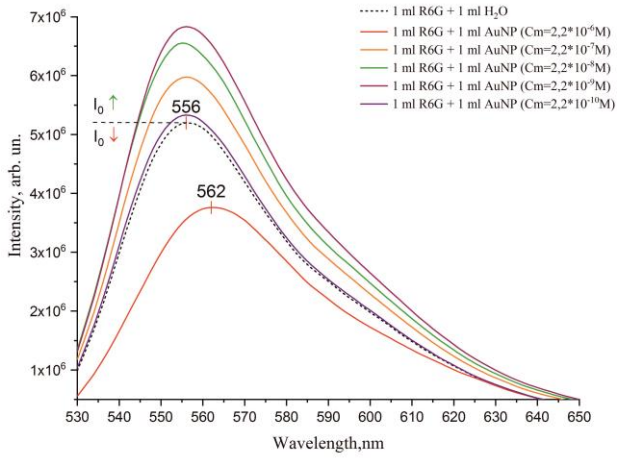

Fig. 8 – (Color online) Fluorescence spectra of the R6G-Au NPs complex where Au NPs are spherical, molar concentration of NPs is variable and R6G concentration is constant at 100 μM.

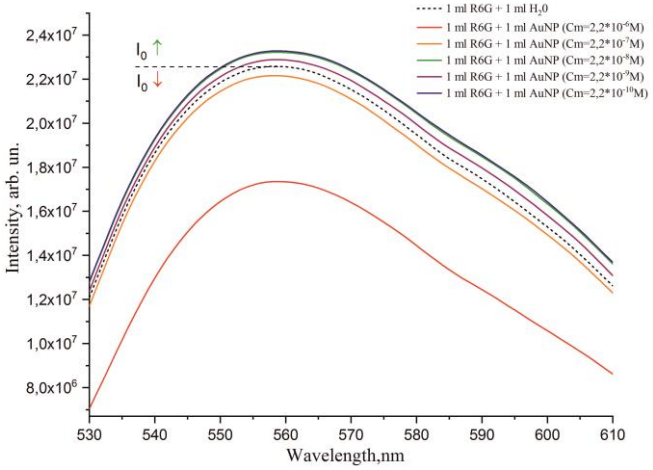

Fig. 9 – (Color online) Fluorescence spectra of the R6G-Au NPs complex where Au NPs are spherical, molar concentration of NPs is variable and R6G concentration is constant at 10 μM.

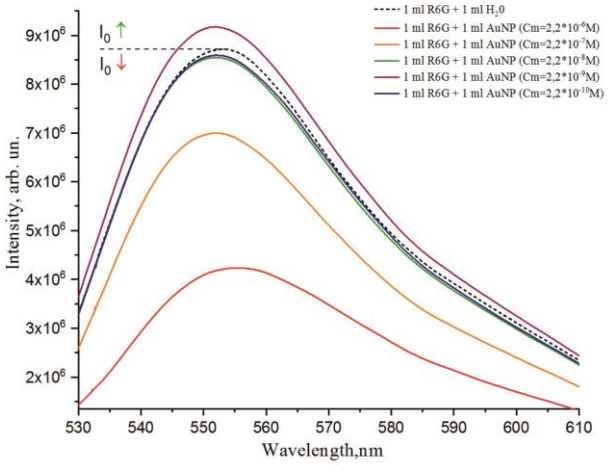

Fig. 10 – (Color online) Fluorescence spectra of the R6G-Au NPs complex where Au NPs are spherical, molar concentration of NPs is variable and R6G concentration is constant at 1 μM.

In the case of gold spheres coated with a SiO_2 shell (Fig. 11 – 14), a smaller red shift was noted, which indicates a larger contribution of scattering from silicon shells and individual silicon NPs. Thus, for R6G concentration of 1000 μM, the shift, as compared to the spheres without a shell, decreased to 3 nm, and for R6G

the concentration of 10 μM it was detected at 4 nm. The uneven character of amplification and extinguishing persisted.

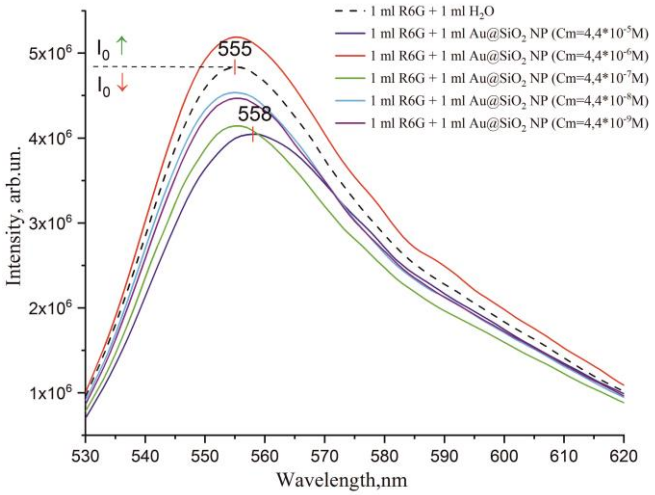

Fig. 11 – (Color online) Fluorescence spectra of the R6G-NPs complex where Au NPs are spherical and coated with SiO_2 shell, NPs molar concentration is variable and R6G concentration is constant at 1000 μM.

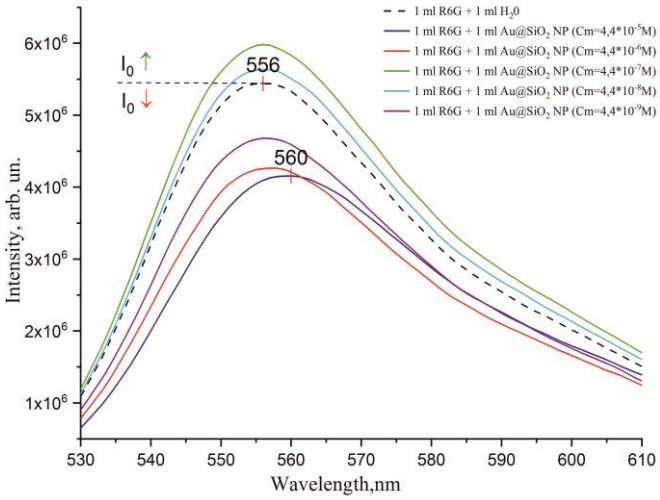

Fig. 12 – (Color online) Fluorescence spectra of the R6G-NPs complex where Au NPs are spherical and coated with SiO_2 shell, NPs molar concentration is variable and R6G concentration is constant at 100 μM.

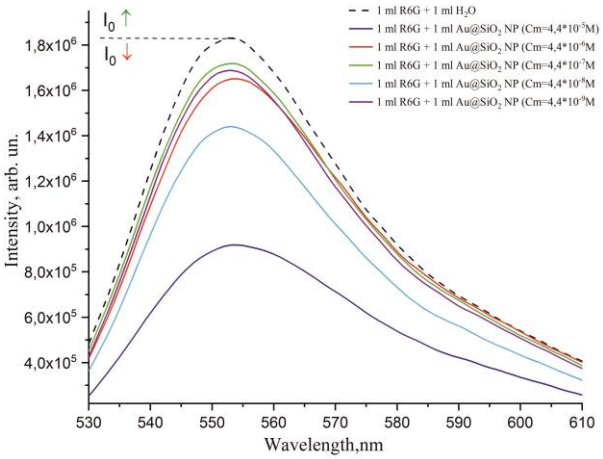

Fig. 13 – (Color online) Fluorescence spectra of the R6G-NPs complex where Au NPs are spherical and coated with SiO_2 shell, NPs molar concentration is variable and R6G concentration is constant at 10 μM.

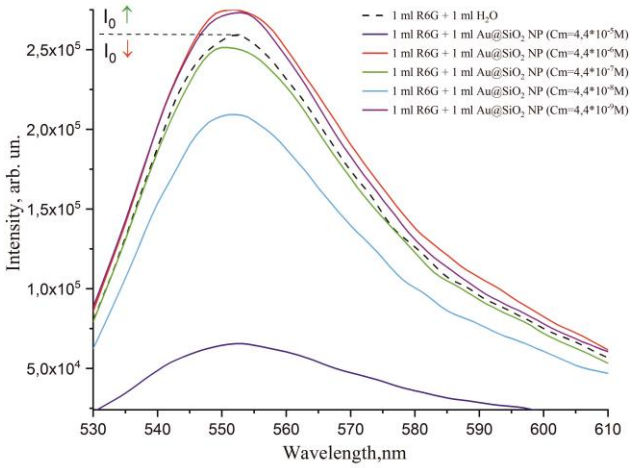

Fig. 14 – (Color online) Fluorescence spectra of the R6G-NPs complex where Au NPs are spherical and coated with SiO_2 shell, NPs molar concentration is variable and R6G concentration is constant at 1 μM.

4. CONCLUSION

The optical properties of R6G-Au NP and R6G-Au@SiO_2 NPs complexes have been studied. Both MEF and quenching effects have been observed. Spectral fluorescent properties of R6G molecules in the complexes with gold NPs with/without SiO_2 shell have

been investigated. FDTD modeling of optical parameters has been carried out. Mesoporous silica nanoparticles (MSNs) have been added into the system for Au@SiO_2 NPs. The influence of SiO_2 shells and MSNs on the photophysical properties of complexes has been shown. The results obtained can be useful for drug loading systems investigations including those for sensory purposes.

Acknowledgements. Chemical synthesis of core/shell nanoparticles was funded by an individual grant in the frame of The Russian Academic Excellence Project «5-100». FDTD modeling and complexes optical properties investigation was funded by RFBR, project number 19-32-90087.

REFERENCES

1. J. Hu, Z. Wang, J. Li, Sensors, **7(12)**, 3299-331 (2007).
2. X. Xie, J. Liao, X. Shao, Q. Li, Y. Lin, Sci. Rep. **7(1)**, 1-9 (2017).
3. V. Amendola, R. Pilot, M. Frasconi, O. M. Maragò, M. A. Iatì, J. Phys.: Cond. Mat. **29(20)**, 203002 (2017).
4. C. Zhu, S. Liang, E. Song, Y. Zhou, W. Wang, F. Shan, J. Liu, Nat. Commun. **9(1)**, 1-7 (2018).
5. B. K. Jena, C. R. Raj, Anal. Chem. **78(18)**, 6332-6339 (2006).
6. K. Sun, Y. Chang, B. Zhou, X. Wang, L. Liu, Int. J. Nanomedicine, **12**, 1905 (2017).
7. Y. Hu, X. Liu, Z. Cai, H. Zhang, H. Gao, W. Z. He, Chem. Mat. **31(2)**, 471-482 (2018).
8. D. Gontero, A. V. Veglia, A. G. Bracamonte, Photochem. Photobiol. Sci. **19(9)**, 1168-1188 (2020).
9. P. L. Stiles, J. A. Dieringer, N. C. Shah, R. P. Van Duyne, Annu. Rev. Anal. Chem. **1**, 601-626 (2008).
10. G. P. Szekeres, J. Kneipp, Front. Chem. **7**, 30 (2019).
11. S. M. El-Bashir, F. M. Barakat, M. S. AlSalhi, J. Lumin. **143**, 43-49 (2013).
12. I. G. Theodorou, Z. A. Jawad, Q. Jiang, E. O. Aboagye, A. E. Porter, M. P. Ryan, F. Xie, Chem. Mater. **29(16),** 6916-6926 (2017).
13. D. Gontero, A. V. Veglia, A. G. Bracamonte, D. Boudreau, RSC Adv. **7(17)**, 10252-10258 (2017)
14. Y. Kobayashi, H. Inose, T. Nakagawa, K. Gonda, M. Takeda, N. Ohuchi, A. Kasuya, J. Colloid Interface Sci. **358(2)**, 329-333 (2011).
15. Aslan K, Wu M, Lakowicz J R, Geddes C D, J. Am. Chem. Soc. **129(6)**, 1524-1525 (2007)
16. P. Reineck, D. Gómez, S. H. Ng, M. Karg, T. Bell, P. Mulvaney, U. Bach, ACS nano **7(8)**, 6636-6648 (2013).
17. C. Li, J. Zhu, Mater. Lett. **112**, 169-172 (2013).
18. H. Xu, J. Colloid Interface Sci. **451**, 101–107 (2015).
19. A. B. D. Nandiyanto, Microporous Mesoporous Mater. **120**, 447–453 (2009).
20. D. J. Swinton, H. Zhang, A. F. Boroujerdi, K. L. Tyree, R. A. Burke, M. F. Turner, T. S. McClary, ACS omega. ***5*(12)**, 6348-6357 (2020).
21. I. Ahmed, E. H. Khoo, O. Kurniawan, E. P. Li, JOSA B. **28(3)**, 352-359 (2011).
22. R. Rajeswari, R. Jothilakshmi, Mater. Sci. Forum. **781**, 33-44 (2014).
23. M. L. Wang, X. L. Jing, L. Shen, Proc. SPIE **8908**, 890807 (2013).
24. I. Kon, A. Zyubin, I. Samusev, JOSA A **37(9)**, 1398-1403 (2020).
25. X. Zhang, C. A. Marocico, M. Lunz, V. A. Gerard, Y. K. Gun'ko, V. Lesnyak, A. L. Bradley, ACS nano ***8*(2)**, 1273-1283 (2014).
26. T. A. Wani, A. H. Bakheit, S. Zargar, M. A. Hamidaddin, I. A. Darwish, PLoS One **12(4)**, e0176015 (2017).
27. D. L. Dexter, J. Chem. Phys **21(5)**, 836-850 (1953).
28. P. F. Gao, Y. F. Li, C. Z. Huang, TrAC Trends in Analytical Chemistry **124**, 115805 (2020).

29. K. J. Chen, C. T. Lin, K. C. Tseng, L. K. Chu, J. Phys. Chem. C **121(27)**, 14981-14989 (2017).
30. S. Raj, G. Adilbish, J. W. Lee, S. M. Majhi, B. S. Chon, C. H. Lee, Y. T. Yu, Ceram. Int. **40(8)**, 13621-13626 (2014).
31. N. K. Pathak, N. Chander, V. K. Komarala, R. P. Sharma, Plasmonics **12(2)**, 237-244 (2017).
32. X. Liu, Colloids Surf. B. **58(1)**, 3-7 (2007).